Synchronization in the connectome: Metastable oscillatory modes emerge from interactions in the brain spacetime network

Joana Cabral [1,2,3*#], Francesca Castaldo[4#], Jakub Vohryzek[2,5], Vladimir Litvak[4], Christian Bick[6,7,8,9], Renaud Lambiotte[8], Karl Friston[4], Morten L. Kringelbach[1,2,3,10], Gustavo Deco[11,12]

[1] Life and Health Sciences Research Institute, School of Medicine, University of Minho, Braga, Portugal
[2] Centre for Eudaimonia and Human Flourishing, Linacre College, University of Oxford, Oxford, United Kingdom
[3] Center for Music in the Brain, Department of Clinical Medicine, Aarhus University, Aarhus, Denmark
[4] Wellcome Centre for Human Neuroimaging, University College London, Queen Square Institute of Neurology, London, United Kingdom
[5] Center for Brain and Cognition, Computational Neuroscience Group, Universitat Pompeu Fabra, Barcelona, Spain
[6] Department of Mathematics, Vrije Universiteit Amsterdam, Amsterdam, The Netherlands
[7] Amsterdam Neuroscience – Systems & Network Neuroscience, Amsterdam, The Netherlands
[8] Mathematical Institute, University of Oxford, Oxford, United Kingdom
[9] Department of Mathematics, University of Exeter, Exeter, United Kingdom
[10] Department of Psychiatry, University of Oxford, Oxford, United Kingdom
[11] Institució Catalana de la Recerca i Estudis Avançats (ICREA), Barcelona, Spain
[12] Department of Neuropsychology, Max Planck Institute for Human Cognitive and Brain Sciences, Germany

Shared first authorship

* Corresponding author:
joanacabral@med.uminho.pt
+351919289649

Summary (150 words)

A rich repertoire of oscillatory signals is detected from human brains with electro- and magnetoencephalography (EEG/MEG). However, the principles underwriting coherent oscillations and their link with neural activity remain unclear. Here, we hypothesise that the emergence of transient brain rhythms is a signature of weakly stable synchronization between spatially distributed brain areas, occurring at network-specific collective frequencies due to non-negligible conduction times. We test this hypothesis using a phenomenological network model to simulate interactions between neural mass potentials (resonating at 40Hz) in the structural connectome. Crucially, we identify a critical regime where metastable oscillatory modes emerge spontaneously in the delta (0.5-4Hz), theta (4-8Hz), alpha (8-13Hz) and beta (13-30Hz) frequency bands from weak synchronization of subsystems, closely approximating the MEG power spectra from 89 healthy individuals. Grounded in the physics of delay-coupled oscillators, these numerical analyses demonstrate the role of the spatiotemporal connectome in structuring brain activity in the frequency domain.

Introduction

The human brain is one of the most complex networks in nature, exhibiting a rich repertoire of activity patterns organized not only in space and time but also in the frequency domain. Indeed, rhythmicity is a central property of brain function – and perhaps of all biotic self organisation: from fast gamma activity in neurons to the life-cycle itself[1-3]. Within the broad range of oscillations emerging at frequencies between 0.05 Hz and 500 Hz, the oscillations detected extracranially with electro- and magnetoencephalography (EEG/MEG) in resting humans typically peak between 0.5 and 30 Hz, being categorized as delta (~0.5-4 Hz), theta (~4-8 Hz), alpha (~8-13 Hz) and beta (~13-30 Hz)[4]. Notably, these oscillations lock in phase over long distances, generating metastable spatial topographies lasting up to a few hundred milliseconds[5-7].

Falling significantly below the range of frequencies generated in local neuronal networks by feedback inhibition (>35Hz, in the gamma frequency range), it is generally agreed that sub-gamma oscillatory activity does not have a purely local origin and is associated to synchronization between distant neural assemblies[8-12]. Notably, there is a correlation between the distance over which synchronization is observed and the frequency of the synchronized oscillations[13,14]. Specific brain circuitries, including among others the thalamocortical loop, have been proposed to play a role in the generation of rhythmic activity[15-17], which appears disrupted in neurological/neuropsychiatric disorders [1,18]. Still, the fundamental mechanisms driving the spontaneous emergence of short-lived spectrally resolved oscillatory patterns remain unclear[8,19-21].

Given the finite axonal propagation speed, interactions between brain areas are intrinsically time-delayed, which can significantly impact network activity in the frequency domain. Indeed, delay-coupled oscillators have been demonstrated to synchronize at frequencies slower than the natural frequency of the oscillators, leading to a form of collective frequency emerging from synchronization mechanisms[22,23]. Briefly, when *N* phase oscillators – with natural frequency ω – are coupled together with a time delay τ, they synchronize at a delay- and interaction-dependent collective frequency Ω given by $\Omega=\omega/(1+K*N*\tau)$, where K is the global coupling strength[22]. However, this phenomenon was demonstrated for networks of phase oscillators coupled to nearest-neighbours with homogeneous delays[22], and it is unclear how it generalizes to more complex real-world systems exhibiting collective rhythmicity, such as the brain.

Computational models have proved helpful for demonstrating how the brain's complex network structure of long axonal projections connecting brain areas – the so-called structural connectome[24] - can *shape* brain activity in space and time[25-33]. Particularly, simulations of oscillatory units interacting in the connectome reveal a critical regime where different subsets of units temporarily synchronize and desynchronize, leading to transiently correlated activity across spatially segregated units[27,34-36]. This reinforces the hypothesis that long-range functional connectivity

between brain areas is driven by synchronization mechanisms[21,37-41]. Importantly, when considering realistic time delays in simulations of phase oscillators coupled in the connectome, periods of increased synchrony are accompanied by increased power at slower frequencies, generating spatially-organized band-limited power fluctuations similar to the ones captured with MEG[35]. While these numerical results reveal the critical role of time delays to generate collective oscillations at reduced frequencies, the underlying mechanistic principle remains unclear. Further, it remains to be verified whether this phenomenon holds in the more realistic setting, wherein local oscillations have fluctuating amplitude, as observed empirically in electrophysiological recordings of neural activity[42,43].

To address these fundamental questions, we build a phenomenological brain network model with realistic connectivity and time delays by representing each node as a Stuart-Landau oscillator operating in the underdamped regime in the presence of background noise[31,32,44,45]. We set the natural frequency of all units in the gamma frequency range (40Hz) and hypothesize that the power spectra of MEG recordings of healthy humans at rest will be approximated in a critical range of parameters where metastable synchronization occurs at reduced collective frequencies following analytic prediction.

Results

Dynamical regimes of the brain network model

The reduced brain network model comprises *N*=90 dynamical units representing anatomically defined brain areas coupled according to the structural connectome with reciprocal (i.e., bidirectional/symmetric) coupling (Figure 1a). Each unit is described by a Stuart-Landau oscillator operating in the underdamped regime, such that when perturbed it decays to a fixed-point equilibrium with a damped oscillation at a natural frequency ω (Figure 1b, see Methods and Supplementary Methods, Section I).

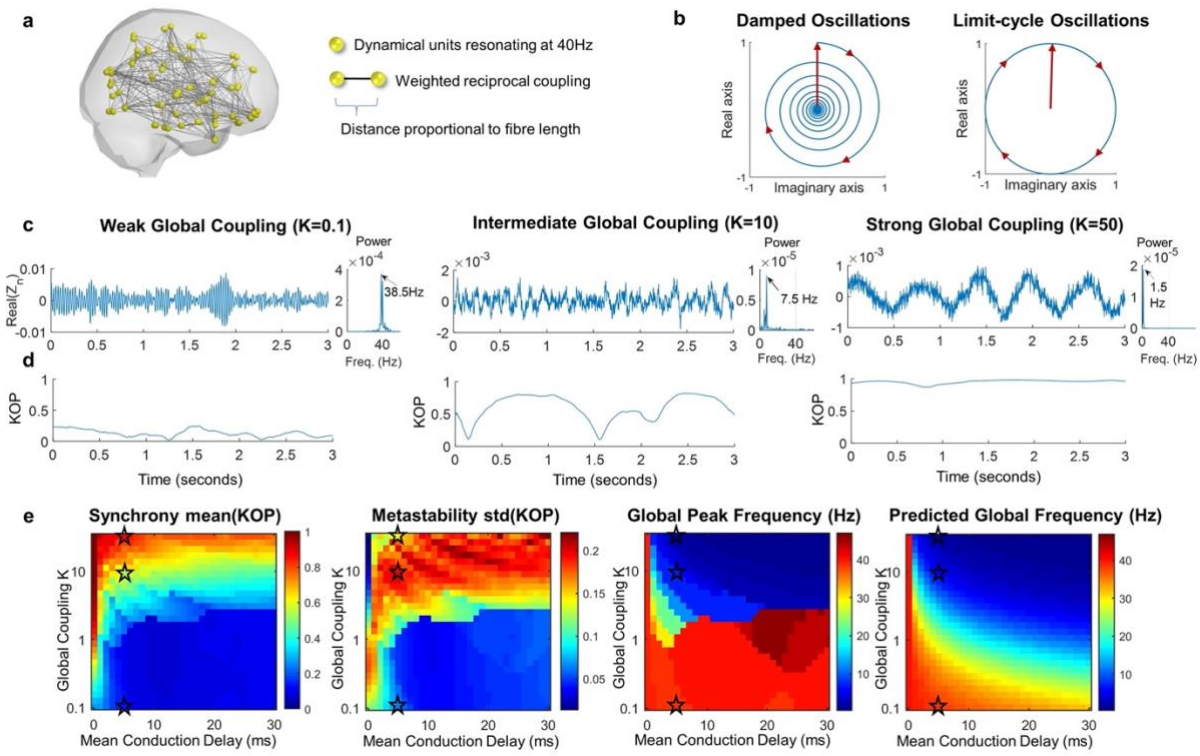

Figure 1 – Collective frequencies emerge from synchronization in the presence of delays. a *– The phenomenological brain network model consists in N=90 nodes representing anatomically defined brain regions with links representing axonal projections between them.* ***b*** *– A Stuart-Landau oscillator in the subcritical regime responding to perturbation (vertical arrow) with an underdamped oscillation (left), in contrast with the super critical regime where the amplitude remains constant (right).* ***c*** *– Simulated signal and corresponding power spectrum in a representative node obtained for three levels of global coupling, with a mean conduction delay of 5 milliseconds and in the presence of white noise. For weak coupling (left) the simulated signal exhibits mostly noise-driven oscillations peaking close to the node's natural frequency. For intermediate coupling (middle), weakly stable synchronization generates transient oscillations at reduced frequencies. For strong coupling (right), global synchronization becomes stable, and all units are entrained in a collective oscillation at a reduced frequency.* ***d*** *– The Kuramoto Order Parameter (KOP) evaluates the degree of phase synchronization of the system. For intermediate coupling, fluctuations in the order parameter are indicative of metastability.* ***e –*** *Simulations were run for 50 seconds over a range of couplings and delays. For each simulation, we report the mean and standard deviation of the KOP (referred to as Synchrony and Metastability[46]) together with the peak frequency of the global signal (i.e.,* $\sum_{n=1}^{N} Z_n$*). The synchronization frequency predicted analytically from* $\Omega = \omega/(1+K*N*\langle\tau\rangle)$ *is reported on the right panel, showing agreement with simulation results for sufficient synchrony.*

To verify that novel frequencies emerge purely from delayed interactions, the natural frequency of all units is set at ω = 40Hz (representing the resonant frequency of isolated neural

masses driven by feedback inhibition) and each unit is perturbed with uncorrelated white noise. The model – represented mathematically by a system of delay coupled differential equations – is solved numerically for two parameter ranges: the global coupling strength, K, which scales all pairwise connections; and the mean conduction delay, $\langle \tau \rangle$, which scales the time delays between units in proportion to the fibre lengths (Figure 1, see Methods for details).

The synchrony degree of the system, evaluated using the Kuramoto Order Parameter (KOP), is modulated by the global coupling strength K: for weak coupling all units exhibit oscillations close to the natural frequency ω and for sufficiently strong coupling all units tend to synchronize at a global collective frequency Ω, which, in the presence of time-delays, is different from the natural frequency ω (Figure 1c-d). In the critical range between incoherence and full synchrony, periods of weakly stable synchronization drive slow fluctuations in the KOP (Figure 1c-d, middle).

Observing the levels of synchrony and metastability across the range of parameters explored (Figure 1e), we find that the critical value of K above which the system can synchronize increases logarithmically with the mean delay, in line with analytic predictions for coupled oscillators with heterogeneous delays[47] (see Supplementary Methods, Section II, Figure S5). When synchronization occurs in the presence of delays, we observe a dramatic decrease in the global peak frequency, closely approximating the analytic prediction given by $\Omega=\omega/(1+K*N*\langle \tau \rangle)$ (Figure 1e) (see Supplementary Methods, Section II, Figure S6). These findings serve to verify that the phenomenon of synchronization at reduced collective frequencies is not restricted to coupled phase oscillators and generalizes to units in the subcritical regime as long as damped oscillations emerge in response to external perturbation (see Supplementary Methods, Section II, Figure S7). Further, it demonstrates that the peak frequency of synchronization can be approximated analytically from global variables such as the natural frequency ω, the number of units N, the coupling strength K, and the mean delay $\langle \tau \rangle$.

Simulations reveal spectral features of human brain activity

One characteristic feature of MEG (and EEG) signals from healthy humans at rest is the transient emergence of oscillations in the alpha frequency range (~8-13Hz), resulting in a peak in the power spectrum whose prominence varies strongly across people (see Figure 2a for the normalized power spectrum of MEG signals from 89 healthy young adults resting with eyes open from the Human connectome Project open-source database; details in *Methods* section).

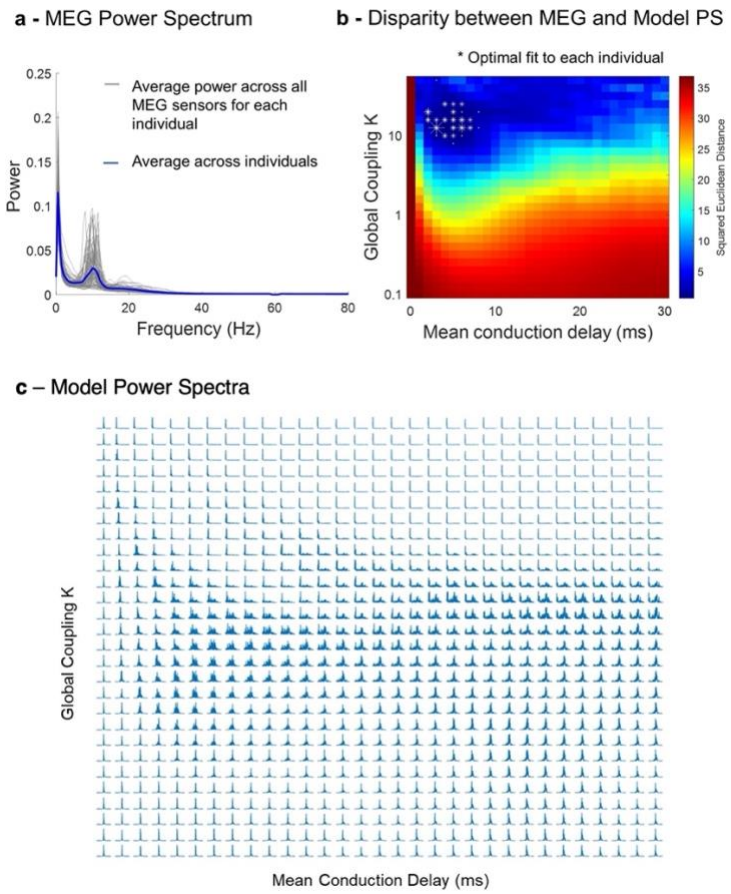

Figure 1 – The model approximates the MEG Power Spectrum (PS) from resting healthy human individuals in a critical range of parameters. a *- MEG power spectra from 89 healthy young adults resting with eyes open from the open-source database of the Human connectome Project. The average power spectrum across individuals is reported in blue.* ***b*** *– Squared Euclidean distance between the MEG power spectrum averaged across all sensors and subjects and the power spectrum of the averaged simulated signals. Asterisks indicate the sets of parameters that optimally approximate the MEG power spectra of each of the 89 individuals (size scaled according to the number of subjects in each point).* ***c*** *– For each pair of parameters (K and* $\langle \tau \rangle$*), the power spectra of the simulated signals (averaged across units and normalized between 0 and 80Hz) is reported.*

We find that the model optimally approximates the average MEG power spectrum of awake resting subjects within the critical region of high metastability where synchronization occurs at reduced collective frequencies (comparing Figure 2b with Figure 1e). In detail, for each pair of model parameters we calculate the squared Euclidean distance between the power spectrum of the simulated signals and the MEG power spectrum averaged across all sensors and all subjects, revealing the greatest disparity when no delays are considered or if the global coupling is too weak (see Methods for details). In addition, we identified the pair of model parameters that optimally approximates the individual MEG power spectra of each of the 89 participants, falling in 24 pairs of parameters (white asterisks in Figure 2b). Notably, this reveals a confined region in parameter space for a range of average delays $\langle \tau \rangle$ of 2 to 8 milliseconds, where slight changes in the coupling strength and conduction speed can account for individual differences in the MEG power spectra, with longer/shorter time delays and stronger/weaker coupling inducing shifts in the peak frequency and modulating the relative power at the peak frequency.

Metastable Oscillatory Modes emerge from weakly stable cluster synchronization

In the range of parameters where the model optimally approximates the power spectrum of MEG signals, fluctuations in the magnitude of the order parameter are driven by metastable cluster synchronization. In other words, when the coupling is strong, but not sufficiently strong to stabilize full synchronization, some subsets of units that are more strongly connected together (i.e., clusters/communities) can engage in partially-synchronized modes that remain stable for a short period in time. Given the presence of time delays, these clusters do not synchronize at the natural frequency of the individual units (40Hz), but instead synchronize at slower cluster-specific collective frequencies, leading to the emergence of metastable oscillatory modes (MOMs) at sub-gamma frequencies.

To detect the occurrence of MOMs and characterize them in space and time, we band-pass filter the simulated signals in 4 frequency bands (delta 0.5-4Hz, theta 4-8Hz, alpha 8-13Hz and beta

13-30Hz). In Figure 3, a coloured shade is added when the amplitude in each frequency band exceeds 5 standard deviations of the amplitude in that same frequency range detected in simulations without delays (see Supplementary Methods, Section IV, Figure S10).

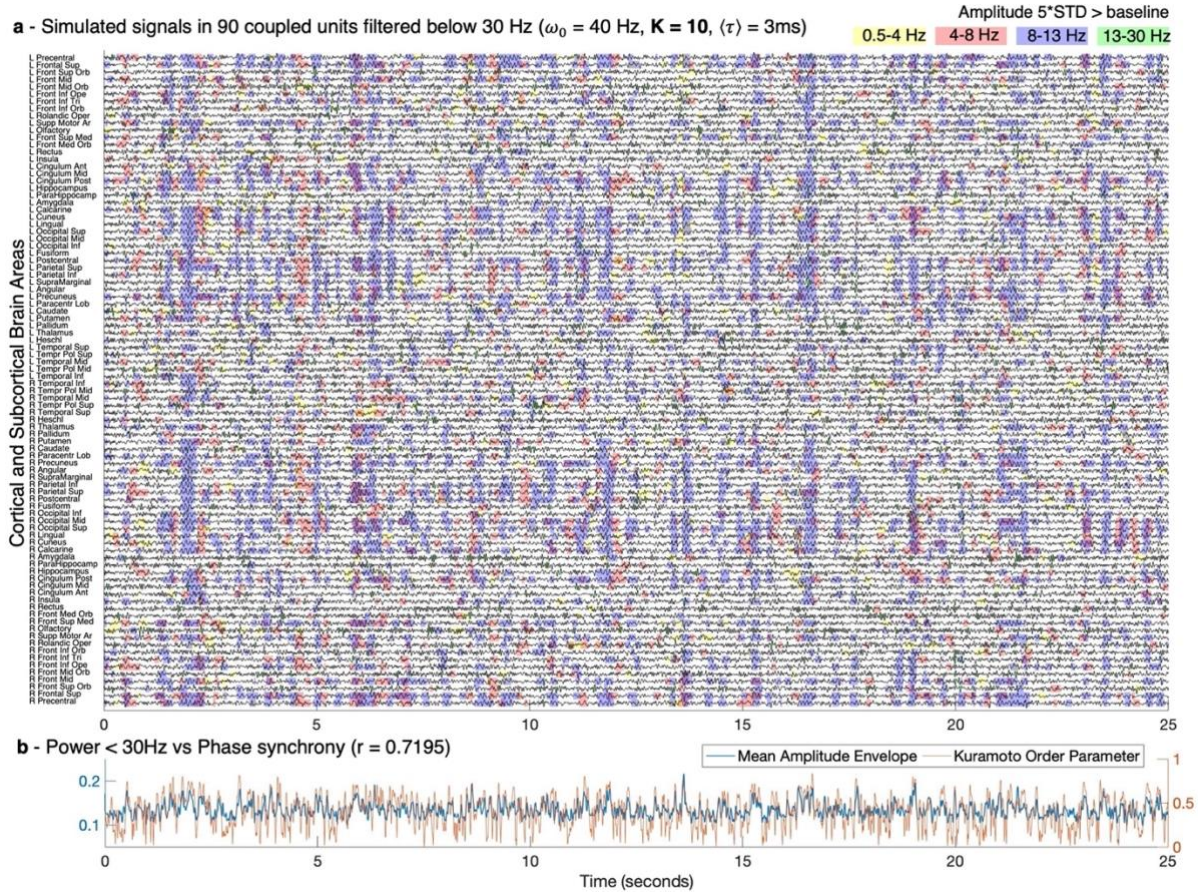

Figure 3. Sub-gamma oscillations emerge from weakly stable cluster synchronization. ***a*** *– An example of the simulated signals in all 90 units plotted over 25 seconds, each representing a brain area from the AAL brain parcellation template, filtered below 30 Hz to highlight the sub-gamma oscillatory activity typically detected with MEG. Shades indicate the time points of increased power in the delta (yellow), theta (red), alpha (blue) and beta (green) frequency bands. For each frequency band, the threshold was defined as 5 standard deviations (STD) of the amplitude – in the same frequency bands – when no delays were considered.* ***b*** *–The mean amplitude envelope (blue) of the filtered signals shown in panel A correlates with r=0.7195 with the phase synchronization evaluated by the Kuramoto Order Parameter (orange, right y-axis).*

As shown in Figure 3, we find that MOMs are structured both in space and in time. Specifically, the units synchronizing together exhibit the simultaneous emergence of an oscillation at the same collective frequency, leading to the vertical alignment of shaded areas, particularly visible

for the alpha frequency range in Figure 3a. Notably, for different sets of parameters, the configuration of Figure 3a changes strongly. Indeed, while for very weak coupling, almost no supra-threshold oscillations are detected (Supplementary Methods, Section IV, Figure S11), for stronger coupling globally synchronized supra-threshold oscillations emerge transiently in the delta band (Figure 4).

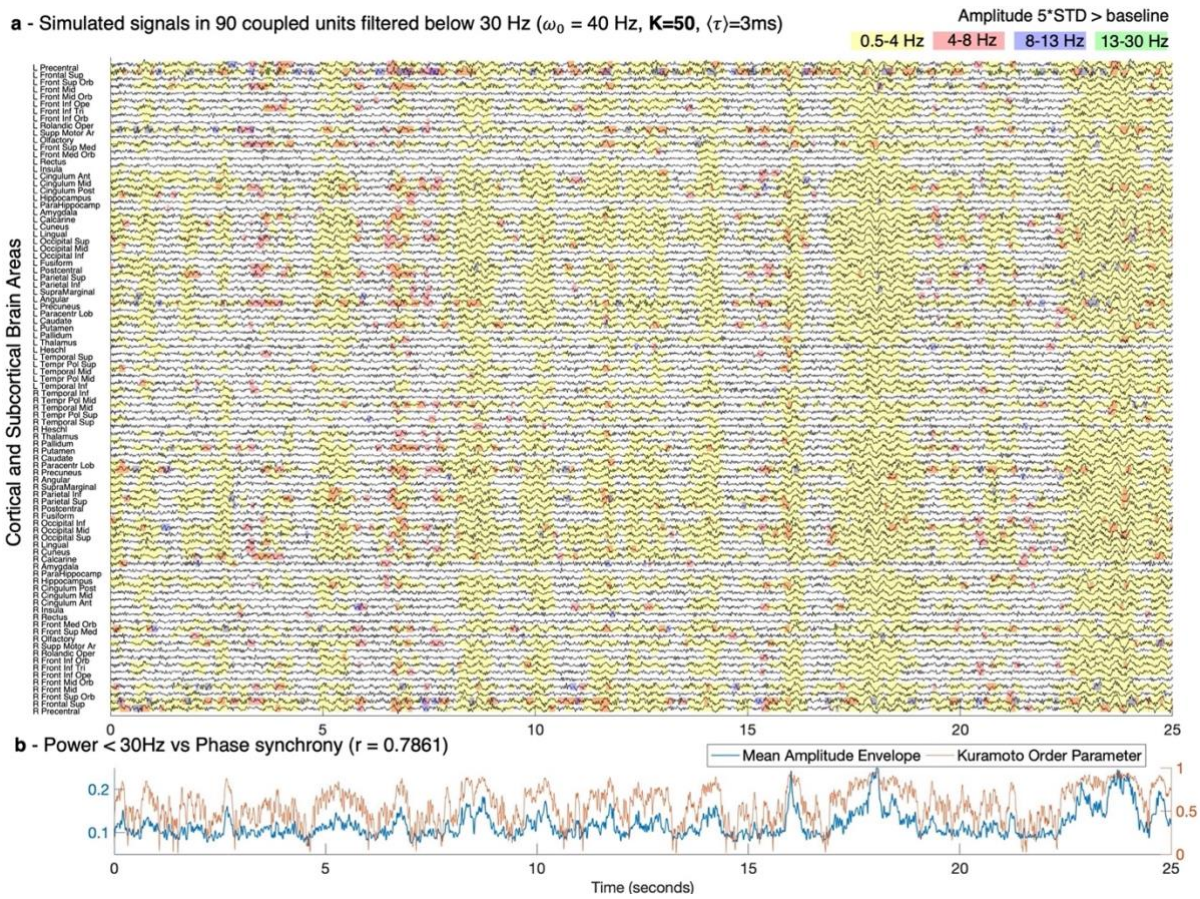

Figure 4 - Global delta waves emerge for strong coupling. ***a*** *– The simulated signals in all 90 units plotted over 25 seconds, each representing a brain area from the AAL brain parcellation template, filtered below 30 Hz to focus on the sub-gamma oscillatory activity typically detected with MEG. Shades highlight the time points of increased power in the delta (yellow), theta (red), alpha (blue) and beta (green) frequency bands. For each frequency band, the threshold was defined as 5 standard deviations (STD) from the amplitude in the same frequency bands when no delays were considered.* ***b*** *–The mean amplitude envelope (blue) of the filtered signals shown in panel A correlates with r=0.7861 with the phase synchronization evaluated by the Kuramoto Order parameter (orange, right y-axis).*

For longer delays, oscillations are detected with less clear temporal alignment between brain areas (Supplementary Methods, section IV, Figure S12). The implicit sensitivity to global model parameters is illustrated in Supplementary Video VS1, where the emergence of supra-threshold oscillations is represented over time in the brain for different sets of parameters.

Furthermore, the power at sub-gamma frequencies is found to correlate strongly with the instantaneous phase synchronization evaluated by the KOP over time (r=0.7195 and r=0.7861 for Figure 3b and Figure 4b correspondingly). This demonstrates that the emergence of oscillations at sub-gamma frequencies in the simulations is modulated by fluctuations in the synchrony degree.

We further define quantitative metrics to characterize the MOMs emerging at different frequency bands for different sets of model parameters in terms of their duration (i.e., consecutive time that the power remains above threshold), their size (i.e., the number of units simultaneous displaying power above threshold) and occupancy (i.e., the proportion of time that the power is detected above threshold) (Figure 5). As can be seen, in the range of parameters where optimal fits to MEG data are obtained (central panel), the alpha MOMs last longer, recruit more units and occur more often. Importantly, we demonstrate that the global parameters such as the coupling strength and the conduction speed can modulate the spatiotemporospectral properties of the whole system in a non-trivial way, while the dynamics at the local level and the underlying structural network remain unchanged.

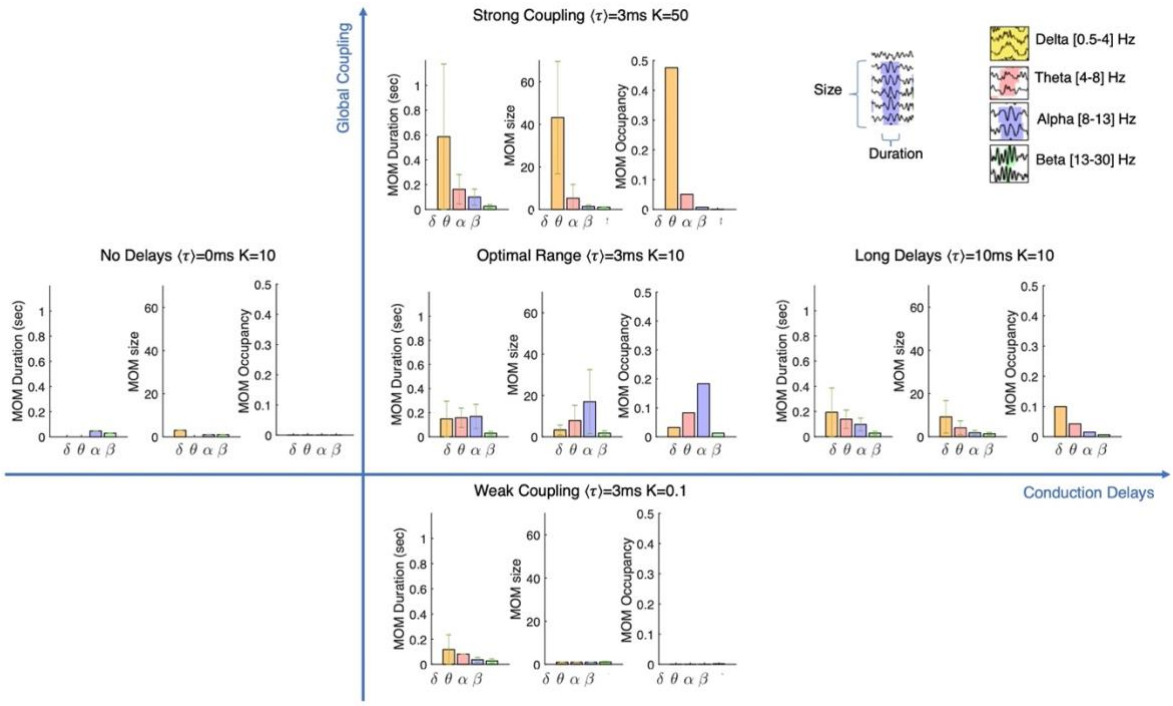

Figure 5. Characterization of metastable oscillatory modes (MOMs) emerging from the system for different sets of parameters. *MOMs are characterized in terms of duration (i.e., consecutive time that the power remains above threshold), size (i.e., the number of units simultaneous displaying power above threshold) and occupancy (i.e., the proportion of time that the power is detected above threshold over the entire simulation), for each frequency band. This demonstrates that the same network structure, i.e., the connectome, can exhibit different oscillatory modes organized in space and in time, depending on global parameters of the system, namely the Global Coupling strength and the Conduction Delays (which are inversely proportional to the conduction speed). In the critical range of parameters (central plot), oscillations in the alpha frequency band emerge more frequently and involve more units. Notably, globally synchronized delta oscillations – as typically observed in states of reduced consciousness – are associated to an increase in the global coupling strength. See also Supplementary Video VS1.*

Spatial patterns of frequency-specific envelope covariance

Finally, we investigate the spatial patterns of connectivity by computing the covariance matrices of the envelopes in each frequency band (Figure 6a) and count the components with eigenvalue (i.e., associated power) above the largest eigenvalue of the same band-specific envelope covariance matrices obtained in the case of no delays (Figure 6b). For weak coupling, the envelope covariance matrices are mostly random in all frequency bands considered and no meaningful component is detected. In the optimal range, the covariance matrices reveal frequency-specific

spatial patterns in all frequency bands, with up to 25 components passing the baseline in the alpha band. In contrast, for strong coupling less spatial patterns are detected in the alpha and beta bands, with most patterns of covariance being detected in the delta band. Finally, for long delays, a large number of modes is detected in all frequency bands, being maximal for the delta range. This illustrates how, given the same underlying spacetime structure (i.e., the matrices of coupling weights *C* and distances *D*), different functional patterns emerge from frequency-specific synchronization.

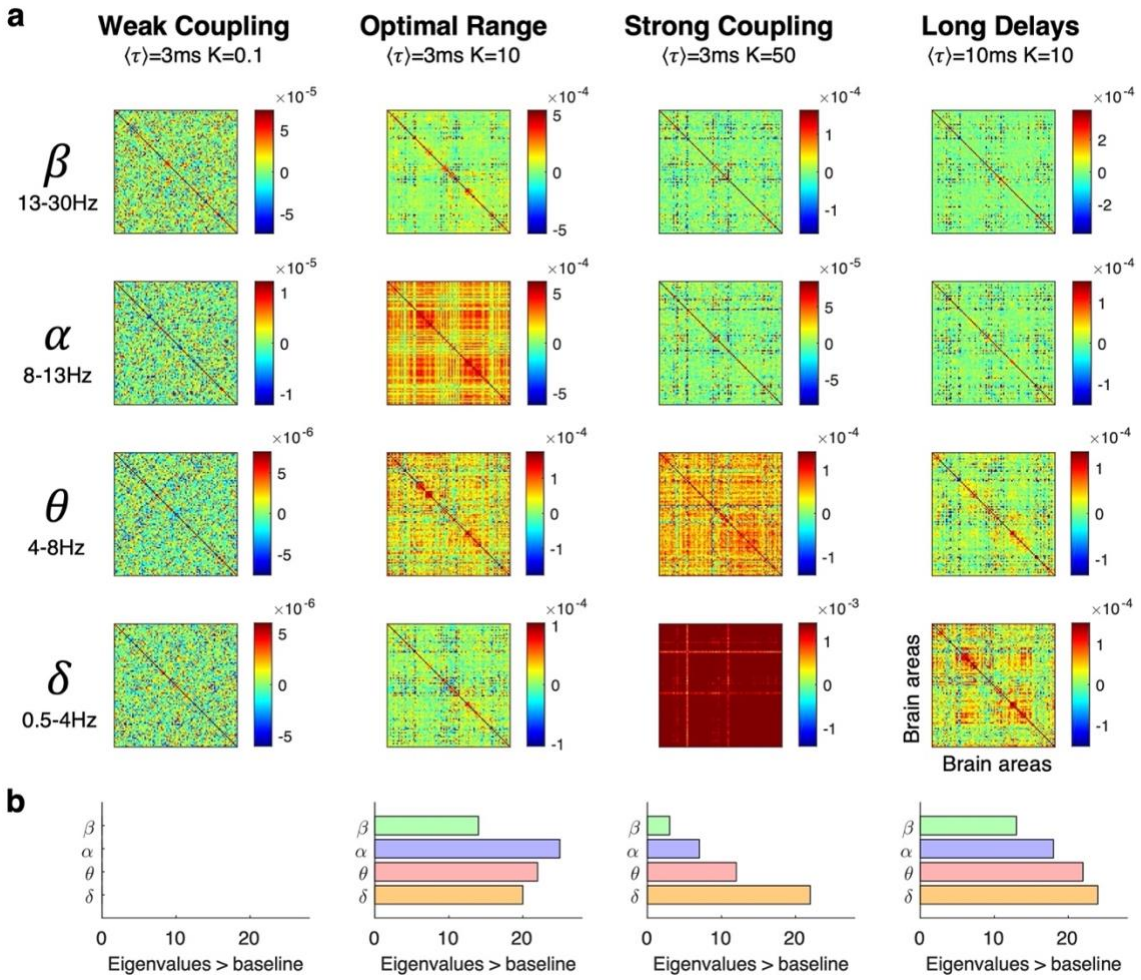

Figure 6. Repertoire of frequency-specific envelope covariance patterns emerging from synchronization in the connectome. a *- For different sets of model parameters, we report the frequency-specific envelope covariance.* ***b*** *– The number of modes in each frequency band is assessed by calculating he number of eigenvalues in each envelope covariance matrix whose magnitude exceeds the largest eigenvalue detected in the case of no delays.*

Discussion

In nature, an extraordinary variety of life processes result from the coordination of interacting dynamical systems, where the collective ensemble engages in functionally-relevant activity patterns that cannot be inferred from the isolated system alone[48-51]. Progress in biophysics implies uncovering the physical mechanisms underlying life processes, grounding the inner complexity of biological systems to universal theoretical principles[52,53].

Here, we describe a universal synchronization mechanism occurring in networks with a complex spacetime structure (i.e., with heterogeneous connectivity and finite conduction speeds) driving the emergence of metastable oscillatory modes at reduced collective frequencies. We propose this mechanism underwrites the formation of macroscopic spatiotemporally organized oscillatory signals recorded with EEG/MEG. Our hypothesis is endorsed using a phenomenological brain network model, reduced to its key essential ingredients to allow efficient numerical approximations to analytic predictions, but at the same time sufficiently complex to allow a fair approximation of MEG spectral features.

The deliberate reductionist perspective inherent in this brain network model is intended to link with theoretical works on delay-coupled oscillatory systems[22,47,54,55]. Towards this end, we consider only N=90 identical units with same natural frequency, same bifurcation parameter and same noise level coupled in the structural connectome. Therefore, we focus solely on the effects of global variables, namely the global coupling K and the mean conduction delay $\langle\tau\rangle$ in the emerging synchronization phenomena. To establish the construct validity of our numerical simulations, we show that the peak synchronization frequency can be approximated by the analytic prediction derived for synthetic networks of coupled Kuramoto oscillators with time delays [22]. Further, in line with theoretical predictions[47,56], we find that the complex spacetime topology of the structural connectome widely expands the critical border between incoherence and global synchrony where fluctuations in the order parameter are indicative of metastability[22]. Despite its simplicity, this model

provides a robust framework to test a theoretically grounded mechanistic scenario for the spontaneous formation of frequency-specific long-range coherence in complex networks.

Building up on these fundamental aspects, additional degrees of complexity can be added to the model, namely by adding more units, tuning the intrinsic frequencies and bifurcation parameter of each brain area, or modulating the level of input noise to mimic local modulatory effects, in order to improve the fitting to empirical data from individuals in different conditions. Further, given the potential universality of this synchronization mechanism, we predict that it can be extended to more realistic biophysical models of neural networks[57], providing a mechanistic interpretation for some of the self-organizing phenomena emerging in systems for which a precise analytic prediction cannot be solved.

Our findings reinforce the idea that conduction delays – often neglected in network models of whole brain activity due to the added complexity – play a crucial role in shaping the frequency spectrum of coupled oscillatory systems. Although the frequency of the oscillations considered herein is relatively fast with respect to the ultra-slow fluctuations (<0.1 Hz) detected with functional Magnetic Resonance Imaging (fMRI), it is important to highlight that metastable synchronization drives power fluctuations on ultra-slow timescales, and therefore, even small time delays can significantly modulate spontaneous activity at ultra-slow time-scales. Importantly, we note that for the model to exhibit the predicted behaviour, the integration step for numerical simulations needs to be sufficiently small (here the simulation results were found to stabilize for $dt \leq 10^{-4}$ seconds), which significantly increases the computation time (here each simulation of 50 seconds lasted approximately 5 hours).

The discovery of multistability in systems of delay-coupled oscillators, initially described in 1999 by Young and Strogatz[54] and extended to heterogeneous delays in 2009 by Lee, Ott and Antonsen[47], was crucial to develop the theoretical hypothesis behind this work, opening grounds to speculate that this phenomenon may be related to the maintenance of the right balance between

integration and segregation in living brains[58,59]. Beyond the range where the model best approximates healthy awake brain activity, we find that higher coupling enhances global order, where the whole brain displays slow coherent oscillations in the delta-range (0.5-2Hz), which nicely approximate the most powerful brain rhythms detected during unconscious states such as slow-wave sleep, coma or anaesthesia. On the other hand, operating at weaker coupling hinders the formation of MOMs at sub-gamma frequencies, altering the spectral profile similarly to what is observed in M/EEG recordings of patients with neuropsychiatric disorders associated to disconnection, such as schizophrenia, where the power in alpha appears to be significantly reduced[60-63]. Such abnormal interactions within cortico-subcortical oscillatory networks may emerge from specific local deregulation or neural circuit disruption[64]. However, how a local change may alter the communication between brain-areas and brain network dynamics remains an open question. Overall, these results are aligned with recent works proposing that spontaneous transitions between multiple space-time patterns on complex networks provide a solid theoretical framework for the interpretation of the non-stationary but recurrent macroscopic patterns emerging spontaneously in brain activity, and ultimately supporting brain function[65,66]. From a technical perspective, it may be surprising that this kind of itinerant dynamics emerges under symmetrical coupling between nodes; in the sense that asymmetric coupling is normally required for breaking detailed balance – and engendering stochastic chaos of the sort described above. However, the dynamics of each node are generated with asymmetric Jacobians, suggesting that symmetry breaking of intrinsic connectivity is a sufficient condition for the nonequilibrium dynamics that characterise real brains.

While metastability appears to be crucial for brain function, the specific role of MOMs to support cognitive functions remains unclear[21,59,67-69]. One possibility is that the areas engaged in a MOM are directly involved in long-range functional integration, but another is that these areas are inhibited by entering in a collective low-energy mode[12,38]. Shedding some light on this open question, we find that synchronization with delays induces not only a shift to slower frequencies but also a decrease in amplitude, in line with theoretical studies reporting amplitude death in systems

with distributed delays[70] (see the vertical axes in Figure 1C). From a 'metabolic' perspective, this shows that MOMs can be approached as 'low energy modes' with respect to high power gamma oscillations, providing a physical explanation for the emergence of the so-called 'idle rhythms'[71]. Although the functional implications of this mechanism are beyond the scope of this work, we expect it will provide fertile grounds for the formulation of novel falsifiable predictions to be further tested. Moreover, these findings give room to further investigations of how local perturbations can affect the spatiotemporospectral dynamics on the macroscopic scale, to gain insight on the mechanisms of action of perturbative strategies such as transcranial magnetic stimulation or deep brain stimulation.

Materials and Methods

Ethics statement

All human data used in this study is from the public repository of the Human connectome Project (HCP)[72] (https://www.humanconnectome.org), which is distributed in compliance with international ethical guidelines.

Structural connectome

The *NxN* matrices of structural connectivity, C, and distances, D, used in the brain network model were computed from diffusion spectrum and T2-weighted Magnetic Resonance Imaging (MRI) data obtained from 32 participants scanned at the Massachusetts General Hospital centre for the Human connectome Project [73] (http://www.humanconnectome.org/).

Briefly, the data were processed using a generalized q-sampling imaging algorithm implemented in DSI Studio (http://dsi-studio.labsolver.org). Segmentation of the T2-weighted anatomical images produced a white-matter mask and co-registering of the images to the b0 image of the diffusion data using SPM12. In each participant, 200,000 fibres were sampled within the white-matter mask. Fibres were transformed into Montreal Neurological Institute (MNI) space using Lead-DBS87[6].

316 The connectivity matrix C was obtained by counting the number of fibres detected between each
317 pair of *N=90* brain areas defined in the Automated Anatomical Labelling (AAL) parcellation scheme[74].

318 Similarly, the distance matrix D was obtained by computing the mean length of all fibres detected
319 between each pair of *N=90* brain areas (see Supplementary Methods section V, Figure S9).

Neuroimaging acquisition and pre-processing

320 We used the human resting-state MEG data publicly available from the Human connectome Project
321 (HCP) consortium, acquired on a Magnes 3600 MEG (4D NeuroImaging) with 248 magnetometers.
322 The resting-state data consist of 89 subjects (mean 28.7 years, range 22–35 years, 41 female/48
323 male, acquired in three subsequent sessions lasting 6 min each).
324 A set of pre-processing pipelines are run on all MEG data prior to further resting-state analysis. To
325 measure the power spectrum of the resting state MEG data at the sensor level, we used the
326 "powavg" pipeline. The continuous data are segmented, Hanning-tapered, Fourier-transformed and
327 the estimated power is averaged over all segments. The power spectrum is represented as FieldTrip
328 structure in a MATLAB file. Notch filters are then applied to the band-pass filtered data to remove
329 the power line noise (cut-off frequencies 59-61 Hz and 119-121 Hz). All the details are extracted and
330 further explained in the HCP reference manual
331 (https://humanconnectome.org/storage/app/media/documentation/s1200/HCP_S1200_Release_Re
332 ference_Manual.pdf).

Brain Network Model

333 The Stuart-Landau (SL) equation (Equation 1) is the canonical form to describe the behaviour of a
334 system near an Andronov-Hopf bifurcation, i.e. exhibiting the birth of an oscillation from a fixed
335 point[39,75]. In other words, it is used to describe systems that have a static fixed point (like a resting
336 spring), but respond to perturbation with an oscillation, which may damped or self-sustained
337 depending on the operating point of the system with respect to the bifurcation (see Supplementary

Methods, Figure Sx). This model allows to designate complex-systems behaviour among several applications, bridging the gap between the simplicity of the Kuramoto model and the extensiveness of the phase-amplitude frameworks[76,77]. It describes how the oscillator behaves both when it is weakly attracted to a limit cycle (displaying only damped oscillations in response to perturbation) and, on the other hand, when it is purely restricted to a limit cycle (oscillations remain self-sustained).

Our analysis is based on a system of N=90 SL oscillators coupled in the connectome, considering both the connectivity strength, C_{np}, and the conduction delays, τ_{np}, between each pair of brain areas n and p. The conduction delays are defined in proportion to the fiber lengths between brain areas, assuming an homogenous condtuction speed v, such that $\tau_{np} = D_{np}/v$, where D_{np} is the length of the fibres detected between brain areas n and p. To simulate how the activity in node n is affected by the behaviour of all other nodes p $(p \in N \wedge p \neq n)$, we describe the interaction between nodes in the form:

$$\frac{dZ_n}{dt} = Z_n[a + i\omega - |Z_n^2|] + K\sum_{p\neq n}^{N} C_{np}\left[Z_p\left(t-\tau_{np}\right) - Z_n(t)\right] + \beta\eta_1 + i\beta\eta_2\,, \forall n \in N, \qquad (1)$$

where the complex variable $Z_n(t)$ describes the state of the nth oscillator at time t. The first term in equation (1) describes the intrinsic dynamics of each unit, the second term describes the input received from coupled units and the last terms represent uncorrelated white noise (see Supplementary Methods, Sections I and II for detailed analysis of the model).

With this approach, we consider that the first term of Eq. 1 represents the natural excitability of neuronal assemblies, where $\omega = 2\pi * f_f$ is the angular frequency, with f_f as the fundamental frequency. For our proof of concept, we set all nodes with identical natural frequency $\omega_0 = 2\pi * 40Hz$, representing the undifferentiated ability of a neural mass to engage in gamma-frequency oscillations.

The parameter a determines the position of the each unit with respect to the limit cycle. For $a > 0$, a stable limit cycle appears via a superciritical Hopf bifurcation, while when a < 0 there is only a stable fixed point at the origin $Z_n = 0$, so the bifurcation point is at a = 0. Importantly, if a is sufficiently close to the bifurcation, the system is still weakly attracted to the limit cycle and damped oscillations emerge in response to external input, with a decay time scaled by a. In this work, we pick a value of $a = -5$ for all nodes, such that a single input drives a damped oscillation decaying after ~1s, approximating the slowest decay time-constants of inhibitory receptors (Figure S4) (τdecay(GABAB) ≈ 500-1000ms). In Supplementary Methods (section II, Figure S7) we show that our results are qualitatively similar for a broad range of a values, both positive and negative, thus demonstrating the generalizability of synchronization at collective frequencies to coupled oscillatory systems with fluctuating amplitude, be they damped or self-sustained. We note that this mechanism only fails when the units have an overdamped response (exponential decay without oscillation), which, in this case, only occurred for $a = -500$. Thus it is of great interest in future research to investigate whether the local bifurcation parameters can be tuned based on sensitive observables to fit the MEG data of different individuals in different conditions.

The second term represents the total input received from other brain areas, scaled by parameter K, which sets the strength of all network interactions with respect to the intrinsic node dynamics. Because we wish to focus on the nonlinear phenomena introduced by time delays, we model the node-to-node interactions using a particular *linear diffusive coupling*, as the simplest approximation of the general coupling function, considering *delayed* interactions. Here, the signal of node n at time t is calculated with respect to the activity of all other nodes p at time $t - \tau_{np}$ (where τ_{np} is the time delay between *n* and *p*), scaled by the relative coupling strength given by C_{np}.

The third term of Equation 1 represents the real and imaginary part of Gaussian noise. In this analysis, the system is perturbed with uncorrelated white noise, where η_1 and η_2 are independently drawn from a Gaussian distribution with mean zero and standard deviation $\beta = 0.001$.

In this framework, our whole-brain network model is purely bottom-up (i.e., not inferred from the MEG data we aim at explaining). For a qualitative comparison with the literature in delay-coupled oscillatory systems [22,47,54], we explore the network dynamics as a function of the coupling strength K and the mean delay $\langle\tau\rangle = \langle D\rangle/v$, where $\langle D\rangle$ is the mean length of all fibres detected between each pair of brain areas. For each set of parameters, the model is solved numerically for 50 seconds with an integration step $dt = 10^{-4}$ seconds.

Kuramoto Order Parameter

To evaluate the global synchrony of the simulated network activity over time, we use the Kuramoto order parameter:

$$R(t)e^{i\Theta(t)} = \frac{1}{N}\sum_{n=1}^{N} e^{i\theta_n(t)} \qquad (2)$$

where $\theta_n(t)$ is the phase of each node, given by the argument of Z_n. The temporal evolution of the Order Parameter $R(t)$ provides an instantaneous measure of the degree of synchrony of the ensemble. Since we add noise in the simulations, we first band-pass filter the signals Z_n around the peak frequency of the ensemble. A steady order parameter indicates a stable solution (be it asynchronous, $\langle R(t)\rangle$~0 or synchronous $\langle R(t)\rangle$~1), whereas fluctuations in the order parameter are indicative of *Metastability*, driven by constant transitions between different weakly stable solutions[57]. For the analysis in parameter space, we take the mean $\langle R(t)\rangle$ as a measure of the global synchronization while the standard deviation $STD(R(t))$ indicates how much $R(t)$ fluctuates in time[46].

Analytic Prediction of Collective Frequency of Synchronization

Previous theoretical studies have shown analytically that coupled oscillatory networks with homogeneous delays can find stable solutions at multiple collective frequencies Ω. Let us consider the Kuramoto transition in a population of phase oscillators defined by Equation 3:

$$\dot{\theta}_n(t) = \omega + K \sum_{p \neq n}^{N} C_{np} sin\left[\theta_p\left(t - \tau_{np}\right) - \theta_n(t)\right], \quad (3)$$

and the fully synchronized, uniformly rotating one-cluster state $\theta_n = \cdots = \theta_N = \Omega t$. Substituting this expression into Equation 3 we obtain [22,23,54,70,78]:

$$\Omega = \omega_0 - K * N * \sin(\Omega\tau) \quad (4)$$

where ω_0 corresponds to the nodes' intrinsic frequency and τ is the homogeneous time delay between nodes. As *K* is increased and full synchrony is approached, the system finds an equilibrium point at the lowest stable solution for Equation 4, which is given by:

$$\Omega_{min} = \omega_0/(1 + K * N * \tau) \quad (5)$$

Note that, for collective oscillations to emerge, the global coupling *K* needs to be sufficiently strong such that the synchronized solutions are at least weakly stable. To approximate the analytic prediction from equation (5), the coupling matrix was normalized by its mean, such that <C>=1.

Model Performance

We perform a parameter space exploration by tuning the two free parameters K and $\langle\tau\rangle$. We choose to increase K exponentially as a power of 10 from 10^{-1} to $10^{1.7}$ in steps of $10^{0.1}$, to ensure a range that covers from weak to strong coupling. $\langle\tau\rangle$ is explored in the range from 0 ms to 30 ms in steps of 1 ms.

We measure the fitting between the empirical sensor MEG PS for each of the 89 subjects and the simulated PS for each pair of parameters as the squared Euclidean distance, resulting in one fitting

value for each subject. This can be regarded as a maximum likelihood procedure under the assumption of Gaussian observation noise.

Metastable Oscillatory Modes

To detect MOMs and characterize them in space and time, we band-pass filter the simulated signals in each frequency band and obtain the corresponding amplitude envelopes using the Hilbert transform for each band. Subsequently, we consider that a node (or brain area) engages in a MOM if the amplitude increases 5 standard deviations above the amplitude in that frequency range. We define the baseline threshold considering the simulations with the optimal K but with zero delays. Since some areas are more coupled together than others, even with “zero delays” these areas exhibit more power in those frequencies that is purely due to noisy interactions. Therefore, we define a different threshold for each node and each band.

Envelope Covariance Patterns

To detect the covariance patterns for each frequency band we calculate the NxN covariance matrices of the NxT envelopes in each frequency band of interest and extract the eigenvalues of that squared matrix, for each band. Our eigenvalues of interest are the ones that for each band are above the largest eigenvalue of the same band-specific envelope covariance matrices obtained in the baseline case - that is null delays and intermediate coupling.

Author contributions

Conceptualization: JC, MLK, GD
Methodology: JC, JV, KF, GD
Investigation: JC, FC
Visualization: JC, FC
Funding acquisition: JC, VL, MLK, GD
Project administration: JC, GD
Supervision: VL, KF, MLK, GD
Writing – original draft: JC, FC
Writing – review & editing: JC, FC, JV, CB, RL, KF, VL, MLK, GD

Competing interests:

Authors declare that they have no competing interests.

Data and materials availability:

All simulations and analysis were performed in Matlab. The codes and materials used in this study are available in: https://liveuclac-my.sharepoint.com/:f:/g/personal/skgtfca_ucl_ac_uk/Er9J06K5b-xCoqaAzRRllp4BSTm7_LWGzNWKoKROXgLJig?e=uiWIHA

which will be deposited in a public database upon acceptance.

Acknowledgments

JC is funded by the Portuguese Foundation for Science and Technology grants UIDB/50026/2020,UIDP/50026/2020 and CEECIND/03325/2017. FC is funded by the EU-project euSNN European School of Network Neuroscience (MSCA-ITN-ETN H2020-860563). The Wellcome Centre for Human Neuroimaging is supported by core funding from Wellcome [203147/Z/16/Z]. JV is supported by the EU H2020 FET Proactive project Neurotwin grant agreement no. 101017716. RL acknowledges support from EPRSC Grants No. EP/V013068/1 and EP/V03474X/1. MLK is supported by the Center for Music in the Brain, funded by the Danish National Research Foundation (DNRF117), and the Centre for Eudaimonia and Human Flourishing, funded by the Pettit Foundation and Carlsberg Foundation. GD is supported by the Spanish national research project (PID2019-105772GB-I00 MCIU AEI), funded by the Spanish Ministry of Science, Innovation and Universities (MCIU), State Research Agency (AEI); HBP SGA3 Human Brain Project Specific grant agreement 3 (945539), funded by the EU H2020 FET Flagship program; SGR Research Support Group (reference 2017 SGR 1545), funded by the Catalan Agency for Management of University and Research Grants (AGAUR); Neurotwin Digital twins for model-driven non-invasive electrical brain stimulation (grant agreement 101017716), funded by the EU H2020 FET Proactive program; euSNN (grant agreement 860563), funded by the EU H2020 MSCA-ITN Innovative Training Networks; The Emerging Human Brain Cluster (CECH) (001-P-001682) within the framework of the European Research Development Fund Operational Program of Catalonia 2014–2020; Brain-Connects: Brain Connectivity during Stroke Recovery and Rehabilitation (201725.33), funded by the Fundacio La Marato TV3; and Corticity, FLAG-ERA JTC 2017 (reference PCI2018-092891), funded by the MCIU, AEI.

Human data were provided by the Human connectome Project, WU-Minn Consortium (Principal Investigators: David Van Essen and Kamil Ugurbil; 1U54MH091657) funded by the 16 NIH Institutes and Centers that support the NIH Blueprint for Neuroscience Research; and by the McDonnell Center for Systems Neuroscience at Washington University.

References

1 Uhlhaas, P. J. & Singer, W. Neural synchrony in brain disorders: relevance for cognitive dysfunctions and pathophysiology. *Neuron* **52**, 155-168 (2006).

2 Engel, A. K., Fries, P. & Singer, W. Dynamic predictions: oscillations and synchrony in top-down processing. *Nature reviews. Neuroscience* **2**, 704-716, doi:10.1038/35094565 (2001).

3 Buzsáki, G. & Draguhn, A. Neuronal oscillations in cortical networks. *Science* **304**, 1926-1929 (2004).

4 Buzsaki, G. *Rhythms of the Brain*. (Oxford University Press, 2006).

5 Baker, A. P. *et al.* Fast transient networks in spontaneous human brain activity. *eLife* **3**, e01867, doi:10.7554/eLife.01867 (2014).

6 Vidaurre, D. *et al.* Spectrally resolved fast transient brain states in electrophysiological data. *NeuroImage* **126**, 81-95, doi:10.1016/j.neuroimage.2015.11.047 (2016).

7 Michel, C. M. & Koenig, T. EEG microstates as a tool for studying the temporal dynamics of whole-brain neuronal networks: a review. *NeuroImage* **180**, 577-593 (2018).

8 Jensen, O., Spaak, E. & Zumer, J. M. in *Magnetoencephalography* 359-403 (Springer, 2014).

9 Sherman, M. A. *et al.* Neural mechanisms of transient neocortical beta rhythms: Converging evidence from humans, computational modeling, monkeys, and mice. *Proceedings of the National Academy of Sciences* **113**, E4885-E4894 (2016).

10 Varela, F., Lachaux, J.-P., Rodriguez, E. & Martinerie, J. The brainweb: phase synchronization and large-scale integration. *Nature reviews neuroscience* **2**, 229 (2001).

11 Hipp, J. F., Hawellek, D. J., Corbetta, M., Siegel, M. & Engel, A. K. Large-scale cortical correlation structure of spontaneous oscillatory activity. *Nature neuroscience* **15**, 884-890, doi:10.1038/nn.3101 (2012).

12 Palva, S. & Palva, J. M. Discovering oscillatory interaction networks with M/EEG: challenges and breakthroughs. *Trends in cognitive sciences* **16**, 219-230 (2012).

13 Schnitzler, A. & Gross, J. Normal and pathological oscillatory communication in the brain. *Nature reviews neuroscience* **6**, 285-296 (2005).

14 Von Stein, A. & Sarnthein, J. Different frequencies for different scales of cortical integration: from local gamma to long range alpha/theta synchronization. *International journal of psychophysiology* **38**, 301-313 (2000).

15 Bhattacharya, S., Cauchois, M. B., Iglesias, P. A. & Chen, Z. S. The impact of a closed-loop thalamocortical model on the spatiotemporal dynamics of cortical and thalamic traveling waves. *Scientific reports* **11**, 1-19 (2021).

16 Freyer, F. *et al.* Biophysical mechanisms of multistability in resting-state cortical rhythms. *The Journal of neuroscience : the official journal of the Society for Neuroscience* **31**, 6353-6361, doi:10.1523/JNEUROSCI.6693-10.2011 (2011).

17 Cabral, J. *et al.* Exploring mechanisms of spontaneous functional connectivity in MEG: How delayed network interactions lead to structured amplitude envelopes of band-pass filtered oscillations. *NeuroImage* **90**, 423-435, doi:10.1016/j.neuroimage.2013.11.047 (2014).

18 Llinás, R. R., Ribary, U., Jeanmonod, D., Kronberg, E. & Mitra, P. P. Thalamocortical dysrhythmia: a neurological and neuropsychiatric syndrome characterized by magnetoencephalography. *Proceedings of the National Academy of Sciences* **96**, 15222-15227 (1999).

19 Vidaurre, D. *et al.* Spontaneous cortical activity transiently organises into frequency specific phase-coupling networks. *Nature communications* **9**, 1-13 (2018).

20 O'Neill, G. C. *et al.* Dynamics of large-scale electrophysiological networks: A technical review. *NeuroImage* **180**, 559-576 (2018).

21 Friston, K. J. Transients, metastability, and neuronal dynamics. *NeuroImage* **5**, 164-171 (1997).

22 Niebur, E., Schuster, H. G. & Kammen, D. M. Collective frequencies and metastability in networks of limit-cycle oscillators with time delay. *Physical review letters* **67**, 2753-2756, doi:10.1103/PhysRevLett.67.2753 (1991).
23 Atay, F. M., Jost, J. & Wende, A. Delays, connection topology, and synchronization of coupled chaotic maps. *Physical review letters* **92**, 144101, doi:10.1103/PhysRevLett.92.144101 (2004).
24 Sporns, O., Tononi, G. & Kotter, R. The human connectome: A structural description of the human brain. *PLoS computational biology* **1**, e42, doi:10.1371/journal.pcbi.0010042 (2005).
25 Honey, C. J., Kotter, R., Breakspear, M. & Sporns, O. Network structure of cerebral cortex shapes functional connectivity on multiple time scales. *Proceedings of the National Academy of Sciences of the United States of America* **104**, 10240-10245, doi:10.1073/pnas.0701519104 (2007).
26 Ghosh, A., Rho, Y., McIntosh, A. R., Kotter, R. & Jirsa, V. K. Cortical network dynamics with time delays reveals functional connectivity in the resting brain. *Cognitive neurodynamics* **2**, 115-120, doi:10.1007/s11571-008-9044-2 (2008).
27 Deco, G., Jirsa, V., McIntosh, A. R., Sporns, O. & Kotter, R. Key role of coupling, delay, and noise in resting brain fluctuations. *Proceedings of the National Academy of Sciences of the United States of America* **106**, 10302-10307, doi:10.1073/pnas.0901831106 (2009).
28 Cabral, J., Hugues, E., Sporns, O. & Deco, G. Role of local network oscillations in resting-state functional connectivity. *NeuroImage* **57**, 130-139, doi:10.1016/j.neuroimage.2011.04.010 (2011).
29 Cabral, J., Kringelbach, M. & Deco, G. Functional Connectivity dynamically evolves on multiple time-scales over a static Structural Connectome: Models and Mechanisms. *NeuroImage* **160**, 84-96, doi:10.1016/j.neuroimage.2017.03.045 (2017).
30 Deco, G. & Kringelbach, M. L. Turbulent-like dynamics in the human brain. *Cell reports* **33**, 108471 (2020).
31 Deco, G. *et al.* Single or Multi-Frequency Generators in on-going brain activity: a mechanistic whole-brain model of empirical MEG data. *NeuroImage*, doi:10.1016/j.neuroimage.2017.03.023 (2017).
32 Deco, G., Kringelbach, M. L., Jirsa, V. K. & Ritter, P. The dynamics of resting fluctuations in the brain: metastability and its dynamical cortical core. *Scientific reports* **7**, 3095, doi:10.1038/s41598-017-03073-5 (2017).
33 Tewarie, P. *et al.* How do spatially distinct frequency specific MEG networks emerge from one underlying structural connectome? The role of the structural eigenmodes. *NeuroImage* **186**, 211-220 (2019).
34 Cabral, J., Hugues, E., Sporns, O. & Deco, G. Role of local network oscillations in resting-state functional connectivity. *NeuroImage* **57**, 130-139, doi:10.1016/j.neuroimage.2011.04.010 (2011).
35 Cabral, J. *et al.* Exploring mechanisms of spontaneous functional connectivity in MEG: how delayed network interactions lead to structured amplitude envelopes of band-pass filtered oscillations. *NeuroImage* **90**, 423-435, doi:10.1016/j.neuroimage.2013.11.047 (2014).
36 Roberts, J. A. *et al.* Metastable brain waves. *Nature communications* **10**, 1-17 (2019).
37 Ponce-Alvarez, A. *et al.* Resting-state temporal synchronization networks emerge from connectivity topology and heterogeneity. *PLoS computational biology* **11**, e1004100, doi:10.1371/journal.pcbi.1004100 (2015).
38 Engel, A. K., Gerloff, C., Hilgetag, C. C. & Nolte, G. Intrinsic coupling modes: multiscale interactions in ongoing brain activity. *Neuron* **80**, 867-886 (2013).
39 Cocchi, L., Gollo, L. L., Zalesky, A. & Breakspear, M. Criticality in the brain: A synthesis of neurobiology, models and cognition. *Progress in neurobiology* **158**, 132-152 (2017).
40 Deco, G. *et al.* Rare long-range cortical connections enhance human information processing. *Current Biology* **31**, 4436-4448. e4435 (2021).

41 Brookes, M. J. *et al.* Measuring functional connectivity using MEG: methodology and comparison with fcMRI. *NeuroImage* **56**, 1082-1104, doi:10.1016/j.neuroimage.2011.02.054 (2011).
42 Buhl, E. H., Tamas, G. & Fisahn, A. Cholinergic activation and tonic excitation induce persistent gamma oscillations in mouse somatosensory cortex in vitro. *The Journal of physiology* **513 (Pt 1)**, 117-126 (1998).
43 Sanchez-Vives, M. V. & McCormick, D. A. Cellular and network mechanisms of rhythmic recurrent activity in neocortex. *Nature neuroscience* **3**, 1027 (2000).
44 Samanta, H. S., Bhattacharjee, J. K., Bhattacharyay, A. & Chakraborty, S. On noise induced poincaré–andronov–Hopf bifurcation. *Chaos: An Interdisciplinary Journal of Nonlinear Science* **24**, 043122 (2014).
45 Selivanov, A. A. *et al.* Adaptive synchronization in delay-coupled networks of Stuart-Landau oscillators. *Physical Review E* **85**, 016201 (2012).
46 Shanahan, M. Metastable chimera states in community-structured oscillator networks. *Chaos* **20**, 013108, doi:10.1063/1.3305451 (2010).
47 Lee, W. S., Ott, E. & Antonsen, T. M. Large coupled oscillator systems with heterogeneous interaction delays. *Physical review letters* **103**, 044101 (2009).
48 Winfree, A. T. Biological rhythms and the behavior of populations of coupled oscillators. *Journal of theoretical biology* **16**, 15-42 (1967).
49 Haken, H. *Information and Self-Organization - A Macroscopic approach to Complex Systems*. (Springer, 1988).
50 Mirollo, R. E. & Strogatz, S. H. Synchronization of pulse-coupled biological oscillators. *SIAM Journal on Applied Mathematics* **50**, 1645-1662 (1990).
51 Strogatz, S. H. & Stewart, I. Coupled oscillators and biological synchronization. *Scientific American* **269**, 102-109 (1993).
52 Pikovsky, A., Kurths, J., Rosenblum, M. & Kurths, J. *Synchronization: a universal concept in nonlinear sciences*. (Cambridge university press, 2003).
53 Strogatz, S. *Sync: The emerging science of spontaneous order*. (Penguin UK, 2004).
54 Yeung, M. K. S. & Strogatz, S. H. Time Delay in the Kuramoto Model of Coupled Oscillators. *Physical review letters* **82**, 648-651 (1999).
55 Earl, M. G. & Strogatz, S. H. Synchronization in oscillator networks with delayed coupling: A stability criterion. *Physical Review E* **67**, 036204 (2003).
56 Wildie, M. & Shanahan, M. Metastability and chimera states in modular delay and pulse-coupled oscillator networks. *Chaos* **22**, 043131, doi:10.1063/1.4766592 (2012).
57 Bick, C., Goodfellow, M., Laing, C. R. & Martens, E. A. Understanding the dynamics of biological and neural oscillator networks through exact mean-field reductions: a review. *The Journal of Mathematical Neuroscience* **10**, 1-43 (2020).
58 Tononi, G., Sporns, O. & Edelman, G. M. A measure for brain complexity: relating functional segregation and integration in the nervous system. *Proceedings of the National Academy of Sciences* **91**, 5033-5037 (1994).
59 Tognoli, E. & Kelso, J. A. The metastable brain. *Neuron* **81**, 35-48, doi:10.1016/j.neuron.2013.12.022 (2014).
60 Cabral, J., Kringelbach, M. L. & Deco, G. Functional graph alterations in schizophrenia: a result from a global anatomic decoupling? *Pharmacopsychiatry* **45 Suppl 1**, S57-64, doi:10.1055/s-0032-1309001 (2012).
61 Cabral, J., Hugues, E., Kringelbach, M. L. & Deco, G. Modeling the outcome of structural disconnection on resting-state functional connectivity. *NeuroImage* **62**, 1342-1353, doi:10.1016/j.neuroimage.2012.06.007 (2012).
62 Schartner, M. M., Carhart-Harris, R. L., Barrett, A. B., Seth, A. K. & Muthukumaraswamy, S. D. Increased spontaneous MEG signal diversity for psychoactive doses of ketamine, LSD and psilocybin. *Scientific reports* **7**, 46421 (2017).

63 Carhart-Harris, R. L. *et al.* The entropic brain: a theory of conscious states informed by neuroimaging research with psychedelic drugs. *Frontiers in human neuroscience* **8**, 20, doi:10.3389/fnhum.2014.00020 (2014).
64 Goriely, A., Kuhl, E. & Bick, C. Neuronal oscillations on evolving networks: dynamics, damage, degradation, decline, dementia, and death. *Physical review letters* **125**, 128102 (2020).
65 Bick, C. Heteroclinic switching between chimeras. *Physical Review E* **97**, 050201 (2018).
66 Ansmann, G., Lehnertz, K. & Feudel, U. Self-induced switchings between multiple space-time patterns on complex networks of excitable units. *Physical Review X* **6**, 011030 (2016).
67 Singer, W. Synchronization of cortical activity and its putative role in information processing and learning. *Annual review of physiology* **55**, 349-374, doi:10.1146/annurev.ph.55.030193.002025 (1993).
68 Rabinovich, M. I., Simmons, A. N. & Varona, P. Dynamical bridge between brain and mind. *Trends in cognitive sciences* **19**, 453-461 (2015).
69 Roberts, J. A. *et al.* Metastable brain waves. *Nature communications* **10**, 1056 (2019).
70 Atay, F. M. Distributed delays facilitate amplitude death of coupled oscillators. *Physical review letters* **91**, 094101, doi:10.1103/PhysRevLett.91.094101 (2003).
71 Ritter, P., Moosmann, M. & Villringer, A. Rolandic alpha and beta EEG rhythms' strengths are inversely related to fMRI-BOLD signal in primary somatosensory and motor cortex. *Human brain mapping* **30**, 1168-1187 (2009).
72 Van Essen, D. C. *et al.* The WU-Minn Human Connectome Project: an overview. *NeuroImage* **80**, 62-79, doi:10.1016/j.neuroimage.2013.05.041 (2013).
73 Setsompop, K. *et al.* Pushing the limits of in vivo diffusion MRI for the Human Connectome Project. *NeuroImage* **80**, 220-233 (2013).
74 Tzourio-Mazoyer, N. *et al.* Automated anatomical labeling of activations in SPM using a macroscopic anatomical parcellation of the MNI MRI single-subject brain. *NeuroImage* **15**, 273-289, doi:10.1006/nimg.2001.0978 (2002).
75 A., A. A., Vitt, A. A. & Khakin, S. E. Theory of oscillators. *Dover Mathematics* (1987).
76 Aranson, I. S. & Kramer, L. The world of the complex Ginzburg-Landau equation. *Reviews of Modern Physics* **74**, 99-143, doi:10.1103/RevModPhys.74.99 (2002).
77 Olinger, D. J. A low-dimensional model for chaos in open fluid flows. *Physics of Fluids A: Fluid Dynamics* **5**, 1947-1951, doi:10.1063/1.858821 (1993).
78 Sethia, G. C., Sen, A. & Atay, F. M. Clustered chimera states in delay-coupled oscillator systems. *Physical review letters* **100**, 144102, doi:10.1103/PhysRevLett.100.144102 (2008).

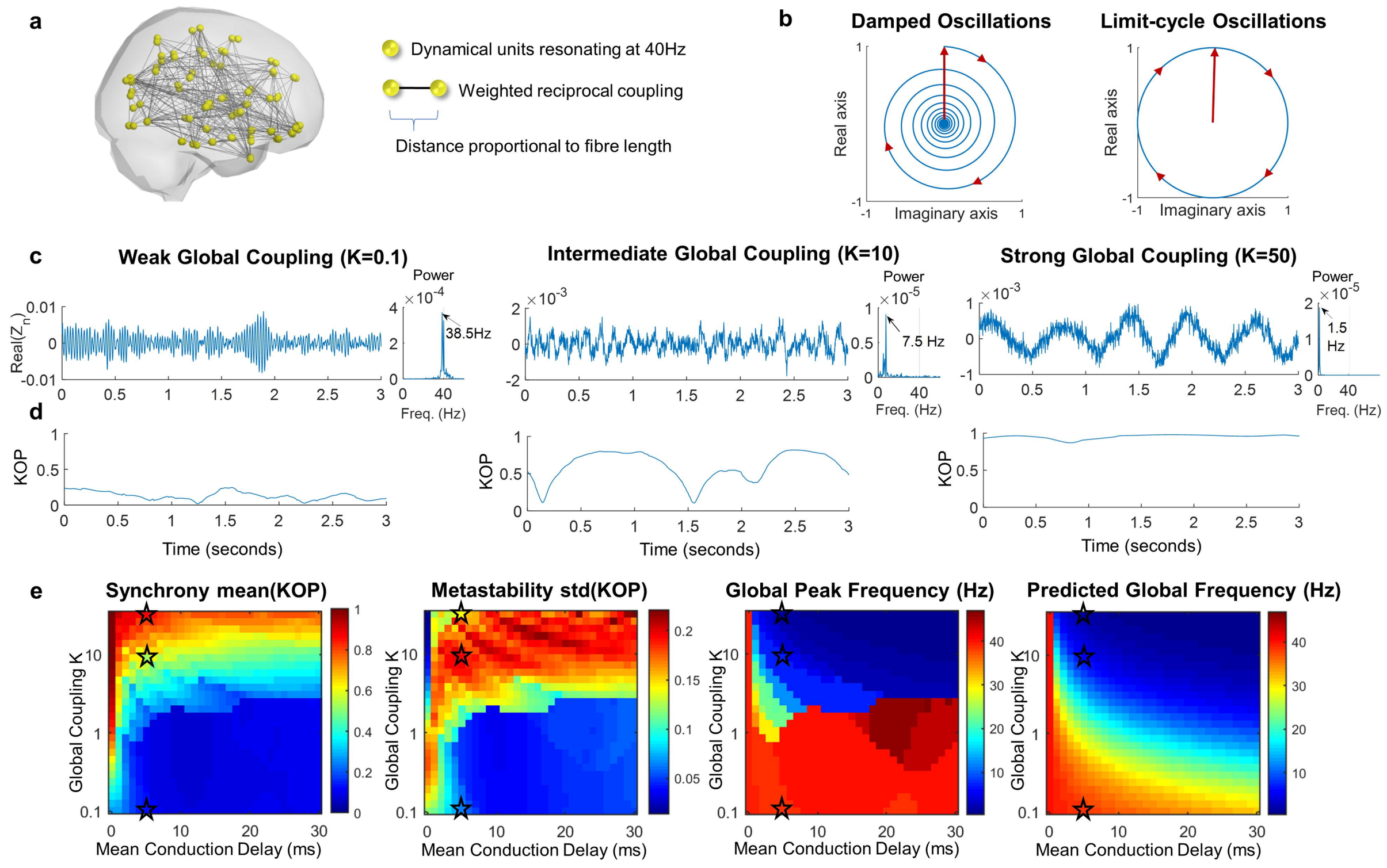
a
Dynamical units resonating at 40Hz
Weighted reciprocal coupling
Distance proportional to fibre length
b
Damped Oscillations
Limit-cycle Oscillations
Real axis
Imaginary axis
c
Weak Global Coupling (K=0.1)
Intermediate Global Coupling (K=10)
Strong Global Coupling (K=50)
Power
38.5Hz
7.5 Hz
1.5 Hz
Freq. (Hz)
d
KOP
Time (seconds)
e
Synchrony mean(KOP)
Metastability std(KOP)
Global Peak Frequency (Hz)
Predicted Global Frequency (Hz)
Global Coupling K
Mean Conduction Delay (ms)

a - MEG Power Spectrum

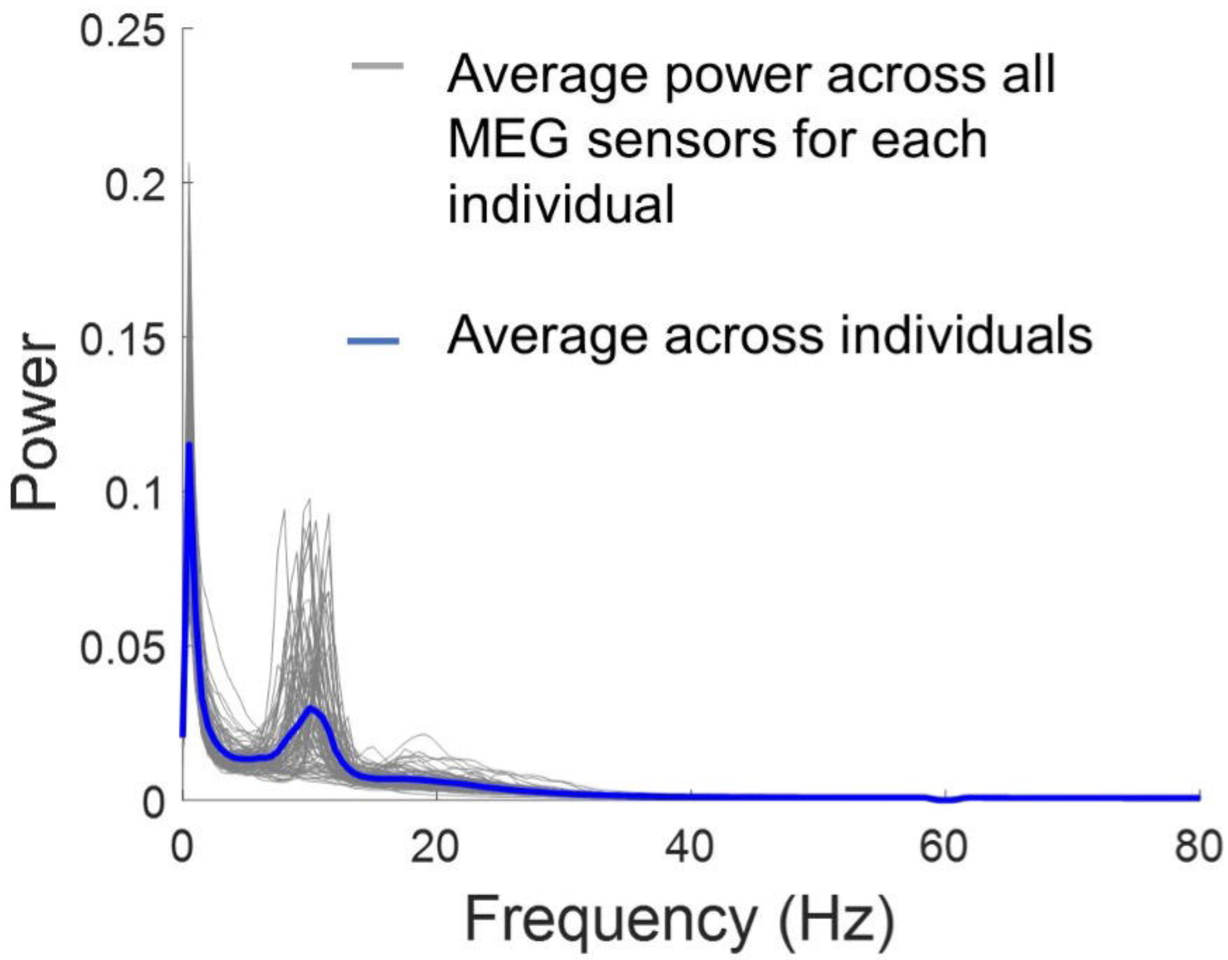

b - Disparity between MEG and Model PS

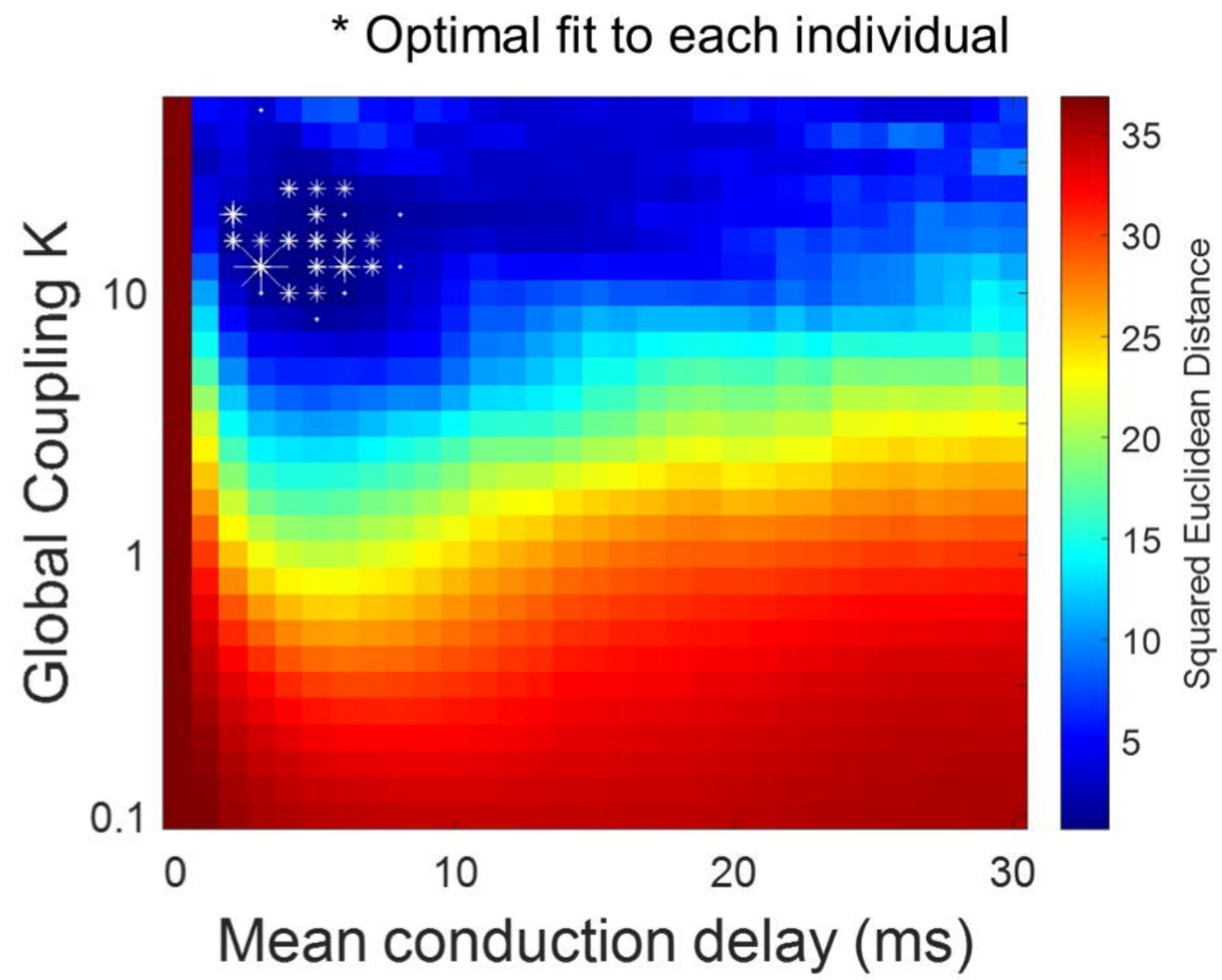

c – Model Power Spectra

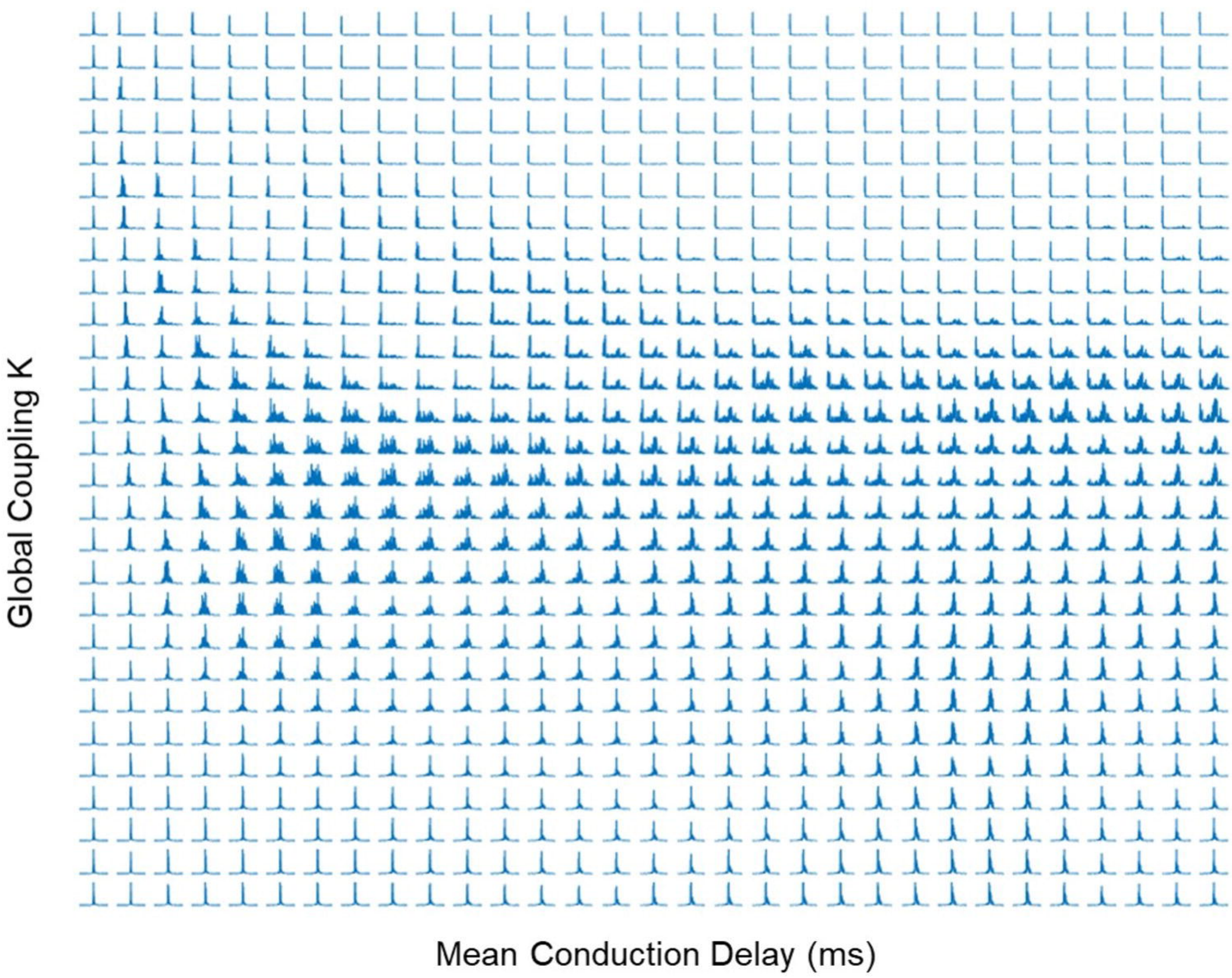

a - Simulated signals in 90 coupled units filtered below 30 Hz (ω_0 = 40 Hz, **K = 10**, $\langle\tau\rangle$ = 3ms)

Amplitude 5*STD > baseline

0.5-4 Hz | 4-8 Hz | 8-13 Hz | 13-30 Hz

Cortical and Subcortical Brain Areas

L Precentral
L Frontal Sup
L Front Sup Orb
L Front Mid
L Front Mid Orb
L Front Inf Ope
L Front Inf Tri
L Front Inf Orb
L Rolandic Oper
L Supp Motor Ar
L Olfactory
L Front Sup Med
L Front Med Orb
L Rectus
L Insula
L Cingulum Ant
L Cingulum Mid
L Cingulum Post
L Hippocampus
L ParaHippocamp
L Amygdala
L Calcarine
L Cuneus
L Lingual
L Occipital Sup
L Occipital Mid
L Occipital Inf
L Fusiform
L Postcentral
L Parietal Sup
L Parietal Inf
L SupraMarginal
L Angular
L Precuneus
L Paracentr Lob
L Caudate
L Putamen
L Pallidum
L Thalamus
L Heschl
L Temporal Sup
L Tempr Pol Sup
L Temporal Mid
L Tempr Pol Mid
L Temporal Inf
R Temporal Inf
R Tempr Pol Mid
R Temporal Mid
R Tempr Pol Sup
R Temporal Sup
R Heschl
R Thalamus
R Pallidum
R Putamen
R Caudate
R Paracentr Lob
R Precuneus
R Angular
R SupraMarginal
R Parietal Inf
R Parietal Sup
R Postcentral
R Fusiform
R Occipital Inf
R Occipital Mid
R Occipital Sup
R Lingual
R Cuneus
R Calcarine
R Amygdala
R ParaHippocamp
R Hippocampus
R Cingulum Post
R Cingulum Mid
R Cingulum Ant
R Insula
R Rectus
R Front Med Orb
R Front Sup Med
R Olfactory
R Supp Motor Ar
R Rolandic Oper
R Front Inf Orb
R Front Inf Tri
R Front Inf Ope
R Front Mid Orb
R Front Mid
R Front Sup Orb
R Frontal Sup
R Precentral

0 5 10 15 20 25

b - Power < 30Hz vs Phase synchrony (r = 0.7195)

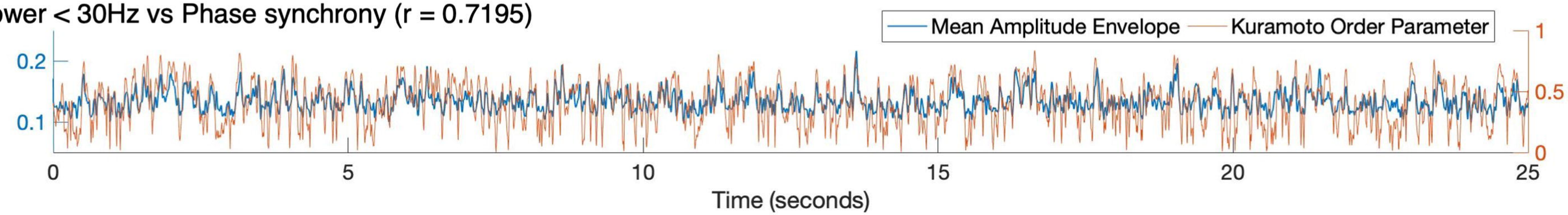

a - Simulated signals in 90 coupled units filtered below 30 Hz (ω_0 = 40 Hz, **K=50**, $\langle\tau\rangle$=3ms)
Amplitude 5*STD > baseline
0.5-4 Hz
4-8 Hz
8-13 Hz
13-30 Hz
Cortical and Subcortical Brain Areas
L Precentral
L Frontal Sup
L Front Sup Orb
L Front Mid
L Front Mid Orb
L Front Inf Ope
L Front Inf Tri
L Front Inf Orb
L Rolandic Oper
L Supp Motor Ar
L Olfactory
L Front Sup Med
L Front Med Orb
L Rectus
L Insula
L Cingulum Ant
L Cingulum Mid
L Cingulum Post
L Hippocampus
L ParaHippocamp
L Amygdala
L Calcarine
L Cuneus
L Lingual
L Occipital Sup
L Occipital Mid
L Occipital Inf
L Fusiform
L Postcentral
L Parietal Sup
L Parietal Inf
L SupraMarginal
L Angular
L Precuneus
L Paracentr Lob
L Caudate
L Putamen
L Pallidum
L Thalamus
L Heschl
L Temporal Sup
L Tempr Pol Sup
L Temporal Mid
L Tempr Pol Mid
L Temporal Inf
R Temporal Inf
R Tempr Pol Mid
R Temporal Mid
R Tempr Pol Sup
R Temporal Sup
R Heschl
R Thalamus
R Pallidum
R Putamen
R Caudate
R Paracentr Lob
R Precuneus
R Angular
R SupraMarginal
R Parietal Inf
R Parietal Sup
R Postcentral
R Fusiform
R Occipital Inf
R Occipital Mid
R Occipital Sup
R Lingual
R Cuneus
R Calcarine
R Amygdala
R ParaHippocamp
R Hippocampus
R Cingulum Post
R Cingulum Mid
R Cingulum Ant
R Insula
R Rectus
R Front Med Orb
R Front Sup Med
R Olfactory
R Supp Motor Ar
R Rolandic Oper
R Front Inf Orb
R Front Inf Tri
R Front Inf Ope
R Front Mid Orb
R Front Mid
R Front Sup Orb
R Frontal Sup
R Precentral
0
5
10
15
20
25
b - Power < 30Hz vs Phase synchrony (r = 0.7861)
Mean Amplitude Envelope
Kuramoto Order Parameter
0.2
0.1
1
0.5
0
0
5
10
15
20
25
Time (seconds)

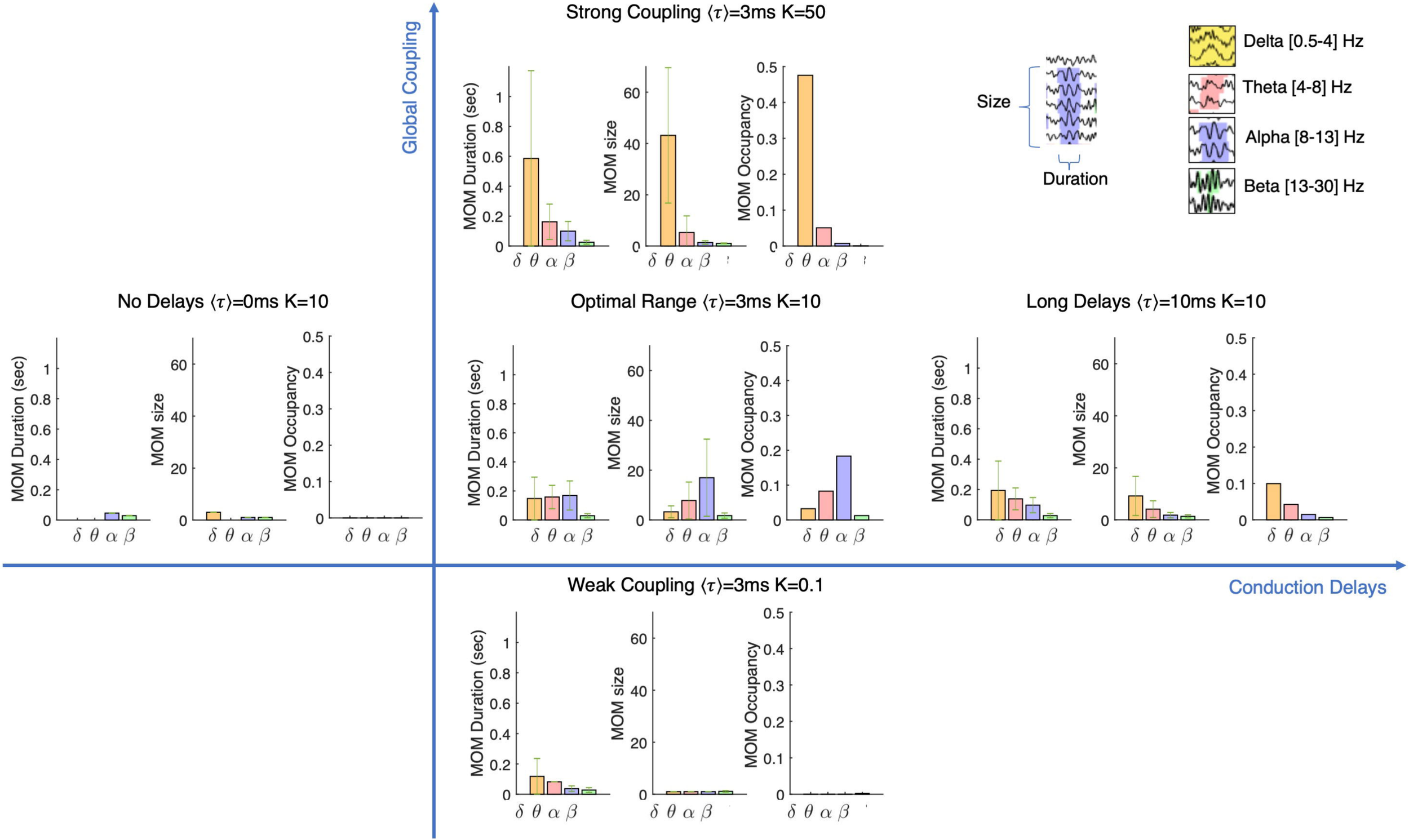
Global Coupling
Conduction Delays
Strong Coupling ⟨τ⟩=3ms K=50
Optimal Range ⟨τ⟩=3ms K=10
Long Delays ⟨τ⟩=10ms K=10
No Delays ⟨τ⟩=0ms K=10
Weak Coupling ⟨τ⟩=3ms K=0.1
MOM Duration (sec)
MOM size
MOM Occupancy
δ θ α β
Size
Duration
Delta [0.5-4] Hz
Theta [4-8] Hz
Alpha [8-13] Hz
Beta [13-30] Hz

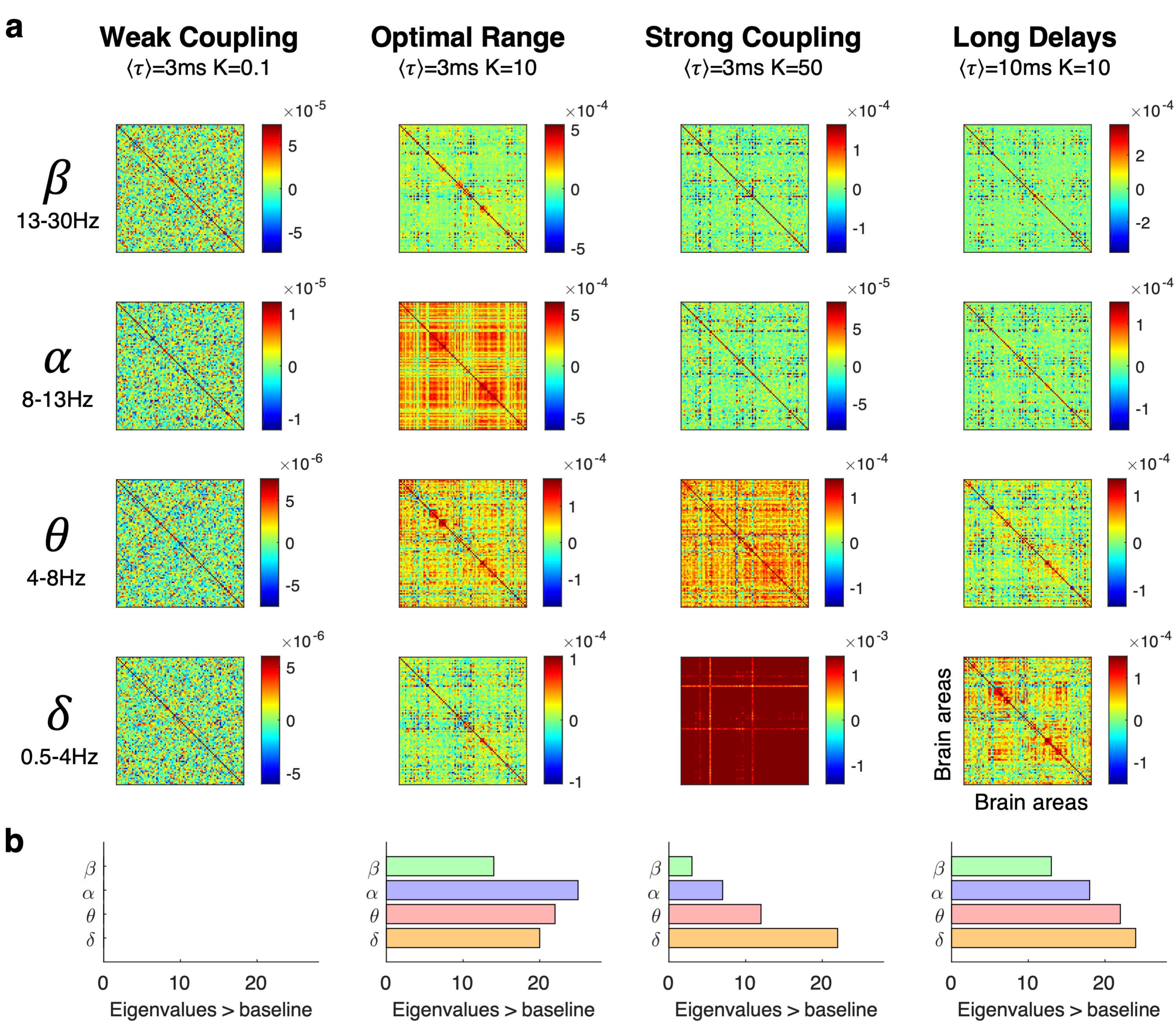
a
Weak Coupling
⟨τ⟩=3ms K=0.1
Optimal Range
⟨τ⟩=3ms K=10
Strong Coupling
⟨τ⟩=3ms K=50
Long Delays
⟨τ⟩=10ms K=10
β
13-30Hz
α
8-13Hz
θ
4-8Hz
δ
0.5-4Hz
Brain areas
Brain areas
b
β
α
θ
δ
0
10
20
Eigenvalues > baseline